

Frequency Domain Filtering SAR Interferometric Phase Noise Using the Amended Matrix Pencil Model

Yandong Gao¹, Shubi Zhang^{1,*}, Kefei Zhang^{2,*} and Shijin Li¹

Abstract: Interferometric phase filtering is one of the key steps in interferometric synthetic aperture radar (InSAR/SAR). However, the ideal filtering results are difficult to obtain due to dense fringe and low coherence regions. Moreover, the InSAR/SAR data range is relatively large, so the efficiency of interferometric phase filtering is one of the major problems. In this letter, we proposed an interferometric phase filtering method based on an amended matrix pencil and linear window mean filter. The combination of the matrix pencil and the linear mean filter are introduced to the interferometric phase filtering for the first time. First, the interferometric signal is analyzed, and the interferometric phase filtering is transformed into a local frequency estimation problem. Then, the local frequency is estimated using an amended matrix pencil at a window. The local frequency can represent terrain changes, thus suggesting that the frequency can be accurately estimated even in dense fringe regions. Finally, the local frequency is filtered by using a linear window mean filter, and the filtered phase is recovered. The proposed method is calculated by some matrices. Therefore, the computational complexity is reduced, and the efficiency of the interferometric phase filtering is improved. Experiments are conducted with simulated and real InSAR data. The proposed method exhibits a better filtering effect and an ideal efficiency as compared with the traditional filtering method.

Keywords: Interferometric phase filtering, interferometric synthetic aperture radar, local frequency estimation, amended matrix pencil, linear window mean filter.

1 Introduction

Interferometric synthetic aperture radar (InSAR/SAR) has become one of the main approaches for DEM inversion and surface displacement monitoring [Song, Guo, Liu et al. (2014)]. Image coregistration, interferometric phase filtering, and phase unwrapping are the main steps for InSAR data processing. Thermal noise, coregistration errors,

¹School of Environment Science and Spatial Informatics, China University of Mining and Technology, Xuzhou, 221116, China.

²SPACE Research Centre, School of Mathematical and Geospatial Sciences, RMIT University, Melbourne, Victoria, 3000, Australia.

* Corresponding Authors: Shubi Zhang. Email: zhangsbi@163.com.

Kefei Zhang. Email: kefei.zhang@rmit.edu.au.

temporal decorrelation, and baseline decorrelation cause noise in the interferometric phase during measurement [Jiang, Ding, Li et al. (2014)]. These noises increase the difficulty of phase unwrapping and DEM inversion and can even lead to unwrapping failure [Yu, Lan, Xu et al. (2017); Yu, Lee, Yuan et al. (2018); Cao, Yu, Lee et al. (2018)]. Therefore, an effective interferometric phase filtering method is of importance.

Interferometric phase filtering aims to filter while avoiding phase loss and resolution degradation. Recently, many interferometric phase filtering methods have been proposed. These methods are mainly divided into two categories: spatial domain methods and frequency domain methods. Among the spatial domain filter methods, multi-look filter [Gao, Liu, Li et al. (2017)] is one of the most commonly used and has best filtering effects but is hindered by several limitations in the fringe density region. The pivoting mean [Lanari, Fornaro, Riccio et al. (1996)] and median filters [Eichel and Ghiglia (1993)] are widely used due to their high efficiency. However, these two methods do not consider the fringe direction and sparse variation. Consequently, interferometric fringes in dense fringes are lost, and the resolution is greatly reduced. In 1998, Lee et al. [Lee, Papathanassiou, Ainsworth et al. (1998)] used a set of optimal directional windows and additive noise models to obtain the least mean square estimation of the interferometric phase. This method can suppress the phase noise while maintaining the phase gradient and its coherence. However, there will still be significant phase loss in the fringe density region. Then, the nonlocal technique is proposed by performing the weighted averaging of similar patches, such as Non-Local Means (NLM) filter [Buades, Coll and Morel (2005)], Probabilistic Patch-Based (PPB) filter [Deledalle, Denis and Tupin (2009)], and Block-matching and 3D transformation-domain collaborative (BM3D) filter [Zhang, Zhang, Zhao et al. (2014); Chierchia, Gheche, Scarpa et al. (2017)]. These nonlocal filtering methods may preserve fringe structures to some extent. However, the computational cost is considerably high due to the similar patches matching in the interferogram, and the precision of the patch similarity is easily influenced by the noise strength. Moreover, spatial domain methods achieve the filtering effect at the expense of the spatial resolution, which is the main drawback of spatial domain methods.

In 1988, Goldstein R M et al. proposed the Goldstein filter, which is regarded as the most classical frequency domain method [Goldstein and Werner (1998)]. However, in view of the global nature of the filtering parameters in the algorithm, the relationship between denoising and phase preservation is difficult to balance. In 2003, Baran et al. used the mean of the coherence in the smoothing window instead of the filtering parameters [Baran, Stewart, Kampes et al. (2003)]. The Goldstein filter can adaptively control the degree of filtering on the basis of the coherence of the interferometric phase. In 2008, considering the biased estimation of coherence, Li et al. [Li, Ding, Huang et al. (2008)] determined the filtering parameters on the basis of all influencing factors, coherence coefficients, and apparent values of the phase standard deviation. In 2014 and 2016, Jiang et al. [Jiang, Ding, Tian et al. (2014)] and Zhao et al. [Zhao, Jiang and He (2016)] improve the Goldstein filter by establishing a parametric model based on the non-biased coherent estimation nonlinear filter, and they are all achieved ideal results. All of these methods improve the classical Goldstein filter to obtain superior filtering effect. However, the suitable parameters are difficult to set. Moreover, the Goldstein filter is hindered by limitations in the fringe density area. To overcome the aforementioned problems, the

slope-compensated filter, based on the local frequency estimation, has attracted an extensive research and discussion. In 2011, Wang et al. proposed a two-step adaptive (TS) filtering method. First, principal phase components are estimated using the frequency spectrum with an adaptive bound and are then removed from the original noisy phase. Thus, a residual noisy phase is obtained. Spatial filtering is conducted on this residual noisy phase image by using four directional masks to obtain a good filtering effect. However, this method produces excessive smoothing and induces phase loss in fringe density regions [Wang, Huang and Yu (2011)]. Originally, Spagnolini used the maximum likelihood (ML) algorithm to estimate the local fringe frequency [Spagnolini (1995)], and subsequently, the modified multiple-signal classification (MUSIC) algorithm [Trouvé, Nicolas and Maître (1998)] and approximate maximum-likelihood algorithm (AML) [Huang and Xu (2008)] were successfully introduced to the interferometric phase filtering. In 2010, Suo et al. [Suo, Li and Bao (2010)] applied local frequency estimation to interferometric phase filtering. They combined the slope compensated and the conventional mean filter. Accurate local unwrapping results were obtained, particularly in the fringe density and low coherence regions. However, those methods are based on the estimation of the maximum likelihood estimation theory, which requires the identification of the peak within the sampling window. This process is time-consuming and thus reduces the efficiency of this method.

This letter proposes a novel interferometric phase filtering method, namely, frequency domain filtering, which is based on an amended matrix pencil and the linear window mean filter. A window centered on a pixel samples the interferometric phase. The assumption is that the frequency of each pixel in the window is consistent, and a signal matrix with the same frequency is established. The matrix is SVD-decomposed. With the large eigenvalue corresponding to the signal vector and the small eigenvalue corresponding to the nature of the noise vector, the sampling matrix is filtered in the first step. The dimension of the filtered sample matrix is reduced, the matrix is SVD-decomposed to the second-step filtering, and the local frequency is estimated. Finally, the estimated frequency is filtered with the linear window mean filter, and the filtered phase value is restored. The window size of filter methods is difficult to set. If the window is too small, the noise will be residued. If the window is too large, the phase will be lost. In this letter, we obtained an optimal window size range by experimental analysis.

This letter is organized as follow. In Section 2, the signal of the interferometric phase is analyzed, and the interferometric phase filtering is transformed into local frequency estimation. Section 3, describes the matrix pencil interferometric phase filtering method and the local frequency linear smoothing model. Section 4, presents two simulated data sets and one real data set, and compares the proposed and traditional methods. Finally, conclusions are summarized in section 5.

2 Interferometric phase signal

The interferometric phase is obtained by the coregistration of the two complex data and can be expressed in a 2D formula as follows [Hua (1992)]:

$$\begin{aligned} x(m,n) &= A(m,n)\exp(j \cdot \phi(m,n)) \\ &= A(m,n)\exp\{j \cdot [\omega|\phi(m,n)| + \varpi(m,n)]\} \end{aligned} \quad (1)$$

where $x(m,n)$ is the complex interferometric phase located at (m,n) , $A(m,n)$ is the amplitude, $\phi(m,n)$ is the measured wrapped phase, $\varphi(m,n)$ is the true phase, $\omega|\cdot|$ is the wrapped factor, and $\varpi(m,n)$ is the interferometric phase noise.

Recovering the real phase from the measured wrapped phase is the most critical step in InSAR data processing. This process is called phase unwrapping. However, the interferometric phase contains noise caused by the thermal noise, coregistration errors, temporal decorrelation, baseline decorrelation, and other factors. This noise increases the difficulty of phase unwrapping and DEM inversion. Thus, an effective interferometric phase filtering method must be used to remove the noise prior to phase unwrapping. The interferometric phase can be generally assumed as a set of sinusoidal signal waves, in which the signal with noise can be written as follows [Rouquette and Najim (2001)]:

$$x(m,n) = \sum_{i=1}^I r_i \exp[j\phi_i + j2\pi(f_{x_i}m + f_{y_i}n)] \quad (2)$$

where I represents the number of 2D spectra. $\{r_i; i=1, \dots, I\}$ is the amplitude, $\{\phi_i; i=1, \dots, I\}$ is the wrapped phase, and $\{(f_{x_i}, f_{y_i}); i=1, \dots, I\}$ is the local frequency of pixel (m,n) . The interferometric phase filtering problem is transformed into a local frequency estimation problem. An interferometric phase signal can be equivalently transformed into a complex matrix as follows:

$$X = \begin{bmatrix} x(0,0) & x(0,1) & \cdots & x(0,N-1) \\ x(1,0) & x(1,1) & \cdots & x(1,N-1) \\ \vdots & \vdots & \ddots & \vdots \\ x(M-1,0) & x(M-1,1) & \cdots & x(M-1,N-1) \end{bmatrix}_{M \times N} \quad (3)$$

From these analyses, we can see the interferometric phase filtering is transformed into a local frequency estimation problem. An interferometric phase signal is expressed in the matrix. In the next section, we introduce the matrix pencil utilized in this study to estimate the local frequency and the linear window mean filter used to obtain the filtered phase.

3 Proposed filtering method

3.1 Amended matrix pencil model

The local frequency of each pixel is difficult to estimate from a large matrix. Thus, a window must be established for estimation. We assume that the frequency of each pixel in the window is consistent. The window size is $(2\ell+1) \times (2\ell+1)$. Thus, the sampling matrix centered on the interferometric phase (a,s) can be expressed as follows:

$$X_{(a,s)} = \begin{bmatrix} X_e(-\ell, -\ell) & X_e(-\ell, -\ell+1) & \cdots & X_e(-\ell, \ell) \\ X_e(-\ell+1, -\ell) & X_e(-\ell+1, -\ell+1) & \cdots & X_e(-\ell, -\ell+1) \\ \vdots & \vdots & \ddots & \vdots \\ X_e(\ell, -\ell) & X_e(\ell, -\ell+1) & \cdots & X_e(\ell, \ell) \end{bmatrix} \quad (4)$$

where $X_e(\ell, \ell)$ is the interferometric phase matrix with noise. By decomposing the signal $X_{(a,s)}$ matrix by SVD-decomposed, we obtain the following equation:

$$X_{(a,s)} = U_s \Sigma_s V_s^H + U_n \Sigma_n V_n^H \quad (5)$$

where U_s and V_s are the eigenvectors corresponding to the large eigenvalues, i.e., the signal vector; and Σ_s is the sum of the large eigenvalues, which is known as the main eigenvalue. U_n and V_n are the eigenvectors corresponding to the small eigenvalues, i.e., the noise signal vector; and Σ_n is the sum of the small eigenvalues, which is known as the nonprincipal eigenvalue. The eigenvector corresponding to the large eigenvalue is needed in the sample signal matrix to achieve the filtering the signal matrix. Therefore, the filtered eigenvalues can be expressed as follows:

$$\bar{\Sigma}_s = \begin{bmatrix} \bar{\alpha}, 0, \dots, 0 \\ [0]_{(2\ell-1) \times 2\ell} \end{bmatrix} \quad (6)$$

where $\bar{\alpha} = \sum_i^l \Sigma_s$, and l is the number of the large eigenvalues. Thus, the first step of filtering the sampling matrix is:

$$\bar{X}_{(a,s)} = U_s \bar{\Sigma}_s V_s^H \quad (7)$$

The sampled signal matrix is dimensionally reduced as follows to further improve the denoising effect:

$$\begin{aligned} \tilde{X}_0 &= \bar{X}(1:2\ell, 1:2\ell) \\ \tilde{X}_1 &= \bar{X}(2:2\ell+1, 1:2\ell) \\ \tilde{X}_2 &= \bar{X}(1:2\ell, 2:2\ell+1) \end{aligned} \quad (8)$$

\tilde{X}_0 is SVD-decomposed, and the sampling matrix is further filtered.

$$\tilde{X}_0 = U_{0s} \tilde{\Sigma}_{0s} V_{0s}^H + U_{0n} \tilde{\Sigma}_{0n} V_{0n}^H \quad (9)$$

where U_{0s} , V_{0s} , and $\tilde{\Sigma}_{0s}$ contain only the main eigenvalue corresponding to the data signal information. U_{0n} , V_{0n} and $\tilde{\Sigma}_{0n}$ are the noise data signals corresponding to small eigenvalues. Thus, the filtered dimensionality reduction dimension matrix is as follows:

$$\begin{aligned}
\vec{X}_0 &= U_{0s}^T \tilde{X}_0 V_{0s} \\
\vec{X}_1 &= U_{0s}^T \tilde{X}_1 V_{0s} \\
\vec{X}_2 &= U_{0s}^T \tilde{X}_2 V_{0s}
\end{aligned} \tag{10}$$

Therefore, the local frequency of the central pixel (a, s) in the sampling window can be obtained by using the following formula:

$$\begin{aligned}
f_{x(a,s)} &= \text{conj}(\vec{X}_1^+ \vec{X}_0) \\
f_{y(a,s)} &= \text{conj}(\vec{X}_2^+ \vec{X}_0)
\end{aligned} \tag{11}$$

where $(f_{x(a,s)}, f_{y(a,s)})$ is the local frequency estimation of the pixel (a, s) ; \vec{X}_1^+ and \vec{X}_2^+ are the pseudo inverse matrices of \vec{X}_1 and \vec{X}_2 ; and $\text{conj}(\cdot)$ is the conjugate factor of the matrix.

3.2 Linear smoothing of local frequency

In this part, we further filter the local frequency and convert the local frequency to the corresponding phase value. First, the local frequency underwent windowed linearization. The size of the linearized window is $(2\ell_m + 1) \times (2\ell_n + 1)$. The linearized matrix can be expressed as follows:

$$\aleph = \left\{ f_{x(a,s)}^{[0:(2\ell_m)]} \right\} \times \left\{ f_{y(a,s)}^{[0:(2\ell_n)]} \right\} \tag{12}$$

The conjugate of the linearized matrix and the sampling window signal data are multiplied to obtain the frequency spreading matrix as follows:

$$\mathfrak{S} = X_{(a,s)} \text{conj}(\aleph) \tag{13}$$

Finally, the filtered phase value is obtained by mean filtering the extended matrix as follows:

$$\hat{X}_{(a,s)} = \text{mean}(\text{mean}(\mathfrak{S})) \times \aleph_{(a,s)} \tag{14}$$

where $\hat{X}_{(a,s)}$ is the final filtered phase value.

4 Experimental results

In this section, we verify the validity of our proposed method by using simulation data experiment and one real data experiment. First, we analyze the optimal window size interval by simulation data experiments and then experiment with the appropriate window size. And we compare the proposed method with Lee filter, pivoting mean filter, Goldstein filter ($\alpha=0.5$), TS filter and maximum likelihood (ML) filter. The number of residuals (NR), the residuals reduction percentage (RRP) and the mean square error (MSE) of the remainder phase are calculated to evaluate the performance of noise reduction and the ability to preserve the local fringe. The phase discontinuity due to noise in the interferogram is defined as the residuals. The principle is to reduce the integral closed curve to a range of 4 adjacent pixel points, and find the sum of the 2π moduli for

the phase difference Δ_k ($k=1,2,3,4$) between the adjacent 4 pixels. In an interferometric phase, the more residuals, the poorer qualities of the interference phase, and vice versa. All experiments in this letter run on a personal computer with Core i7-6700HQ CPU and MATLAB (R2016b). The formula for MSE [Suo, Li and Bao (2010)] is as follows:

$$MSE = E \left[\left| \arg(\exp(j\hat{\phi} - j\phi_{ideal})) \right|^2 \right] \quad (15)$$

4.1 Analysis of window size

The size of window is one of the important parameters that affect the filtering algorithm. In this paper, we use simulation data experiments to determine the optimal window size range. Fig. 1 shows the simulation data used to determine the optimal window size. We test the proposed method with window sizes of 3×3 , 5×5 , 7×7 , 9×9 , 11×11 , 13×13 , 15×15 , 17×17 , and 19×19 . We also determine the selection interval of the optimal window according to the MSE of the remainder phase, NR, and filtering time. Fig. 2 shows the test results of the window size selection. The MSE is enlarged 100 times, and the number of residual points is reduced by 100 times to facilitate the expression. As shown in Fig. 2, the time increases with the increasing window size. The NR drops rapidly with the increasing window size, and the number of residual points becomes zero when the window size reaches a value. This phenomenon occurs because the number of calculated samples in the window increases with the increase in window size. Hence, when the window size is large enough, the number of residual points becomes zero. However, the MSE changes in a U-shape manner when the window size changes because the number of samples can increase with the increase in the window size. Excessive window sizes can lead to phase loss, thereby reducing the filtering accuracy. Fig. 2 reveals that the optimal window size is 7×7 . However, this window size has a small number of samples and thus has poor filtering effect in the fringe density regions. Therefore, the window sizes within the two red dashed lines [7×7 , 9×9 , 11×11 , 13×13] are the optimal window selection interval. We can select the window size according to the actual situation.

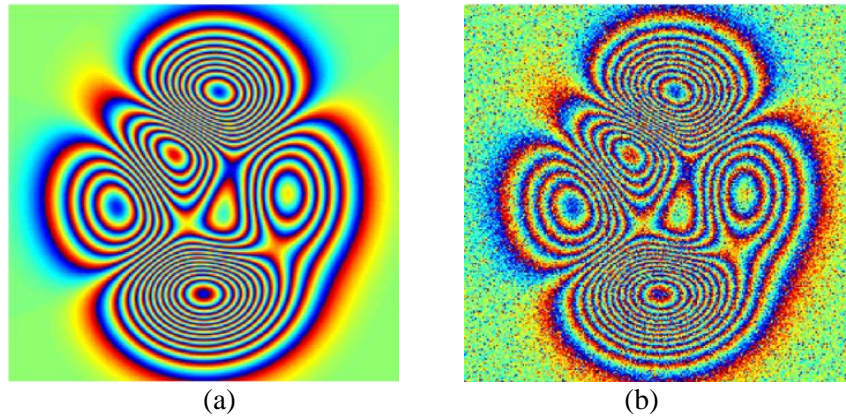


Figure 1: The simulated data used for window selection. (a) The simulated wrapped phase without noise; (b) The simulated wrapped phase with 0.65 rad^2 noise

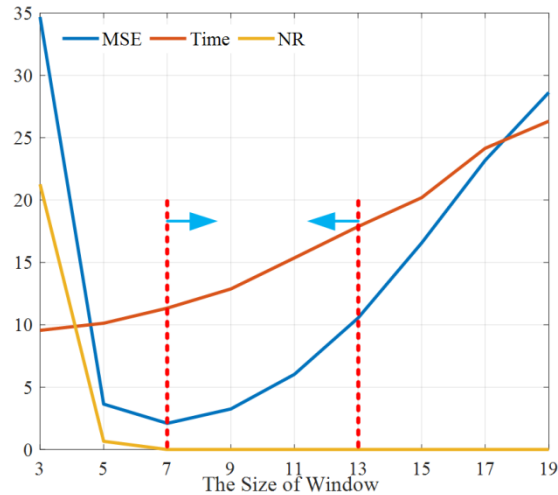


Figure 2: The linear relationship between window size and MSE, Time, NR

4.2 Simulated dataset

The simulation data of Fig. 1 are tested in this part. Tab.1 shows 3693 residuals in the original phase. The window size of all filtering methods in the simulation experiment is set to 7×7 to compare their performance. As shown in Fig. 3 and Table 1, the Lee filter removes 87.11% of the residuals. The MSE of the Lee filter is 0.1301 rad^2 , however, a significant data loss occurs in dense fringe regions. The pivoting mean filter has the highest efficiency, but the result of pivoting mean filter is the worst. The MSE is 1.0698 rad^2 . A total of 342 residuals are found after Goldstein filtering, and 90.74% of these residuals have been removed. The filtering time of the Goldstein method is 7.4269 s. However, a significant phase loss occurs in the dense fringe regions. TS filtering can obtain good filtering accuracy. Its MSE is 0.0208 rad^2 , and only 6 residuals are found after filtering. However, the fringe edge protection ability of this method is poor, and there is a significant excessive smoothing phenomenon. The ML filter accuracy is the same as that of our proposed method and achieved the ideal 100% denoising. Particularly in dense fringe regions, both methods can achieve good denoising effect. The proposed method only uses the 11.0129 s filter and improves the efficiency by 78.91% compared with the ML filter. The MSE values indicate that the ML filter and the proposed method are superior over the other methods except TS filter. However, the efficiency of our proposed method is considerably better than that of the ML filter. In addition, the fringe edge protection ability of the proposed method is better than that of the TS filtering method. The simulated data experiment proves that the proposed method has better filtering effect than the traditional methods.

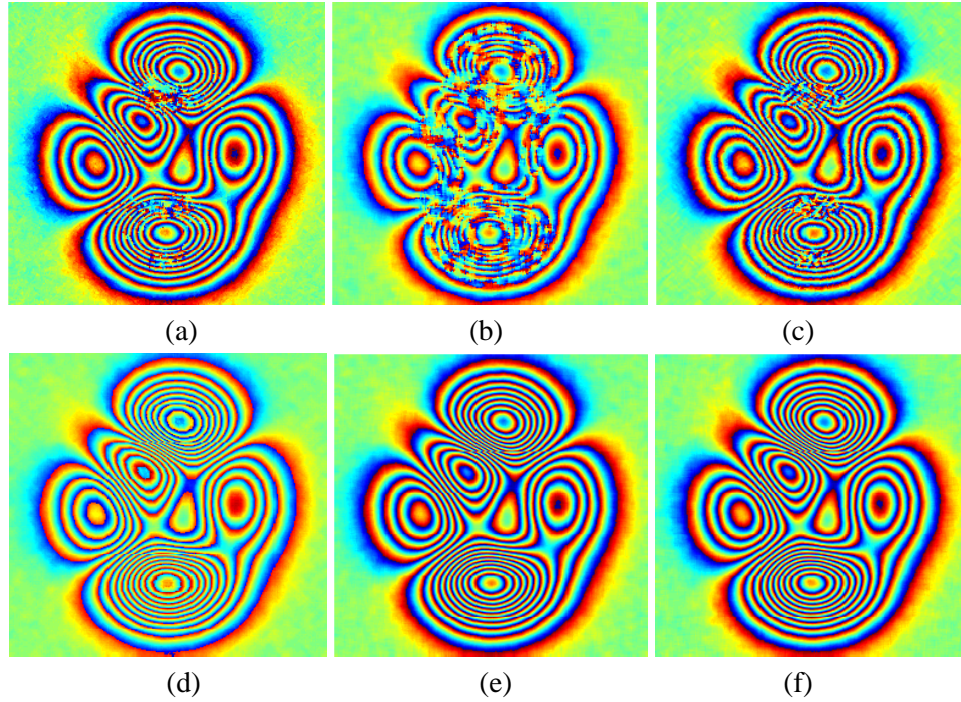


Figure 3: Filtered results of simulated data. The size of simulated data is 256×256 pixels. (a) Lee filter. (b) Pivoting mean filter. (c) Goldstein filter ($\alpha=0.5$). (d) TS filter. (e) ML filter. (f) The proposed method

Table 1: Evaluation results of simulation data

Method	MSE/rad ²	NR	RRP	Time/seconds
Original phase	0.6500	3693	-	-
Lee filter	0.1301	476	87.11%	17.7819
Pivoting mean filter	1.0698	812	78.01%	0.4546
Goldstein filter	0.1779	342	90.74%	7.4269
TS filter	0.0208	6	99.84%	4.4759
ML filter	0.0192	0	100%	52.2086
The proposed filter	0.0212	0	100%	11.0129

4.3 Real dataset

In this section, one set of experimental TanDEM SAR data is used for InSAR processing. The real data is the TanDEM data in the Himalayas, China. Fig. 4 shows the set of experimental data. The range of this data is 1000×1000 pixels. The data was obtained on September 7, 2012. The master image and the slave image are registered, and an interferometric phase is generated. The interferometric phase is flattened to reduce fringe density. Then, the dataset is processed by the Lee filter, pivoting mean filter, Goldstein

filter ($\alpha=0.5$), TS filter, ML filter and the proposed method. From Section 4.1, the terrain of the real data is complex. Thus, the window size for all filtering methods is set to 13×13 in this experiment.

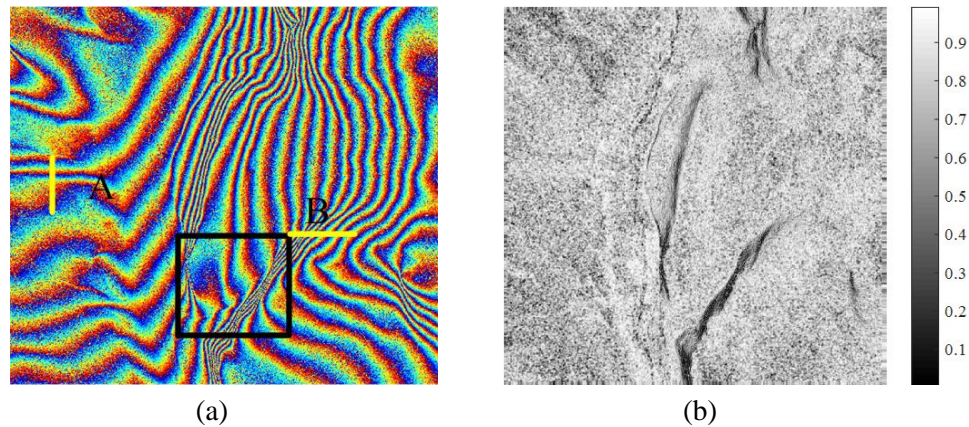


Figure 4: Experimental Real InSAR Dataset: (a) Original interferogram; (b) Corresponding coherence map

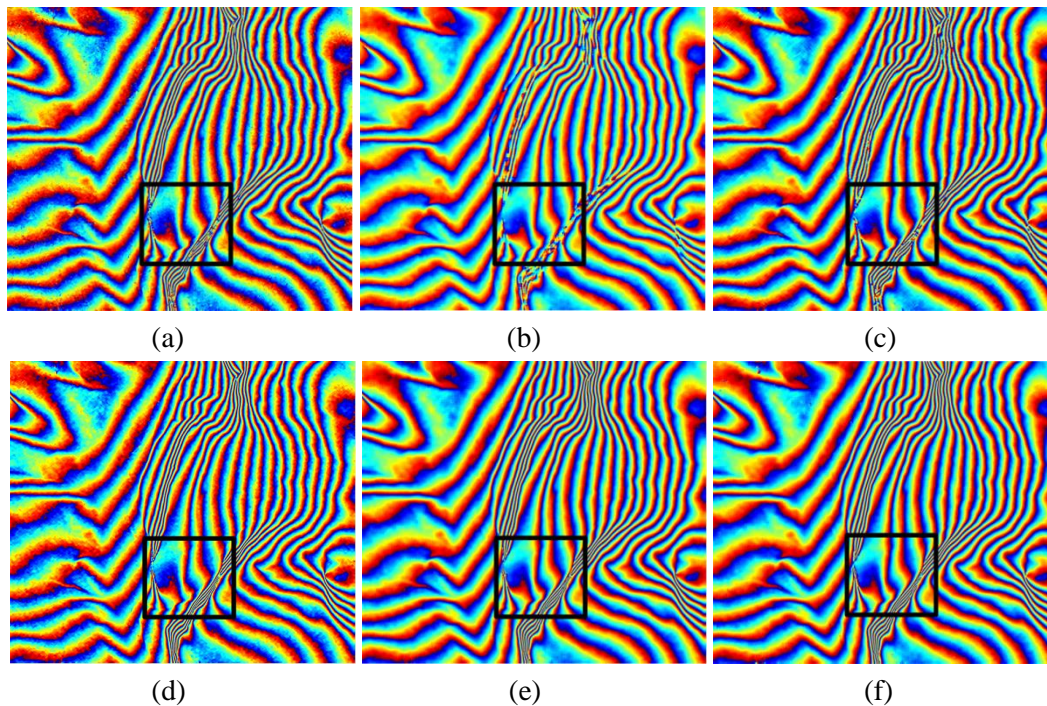


Figure 5: Filtered results of real data. (a) Lee filter. (b) Pivoting mean filter. (c) Goldstein filter ($\alpha=0.5$). (d) TS filter. (e) ML filter. (f) The proposed method

Table 2: Evaluation results of real data

Method	NR	RRP	Time/seconds
Original phase	59715	-	-
Lee filter	1151	98.07%	255.8603
Pivoting mean filter	314	99.47%	12.6940
Goldstein filter	245	99.58%	139.4579
TS filter	124	99.79%	54.9642
ML filter	170	99.71%	850.2027
The proposed filter	106	99.82%	266.3910

As shown in Fig. 5 and Tab. 2, the Lee filter can remove 98.07% of the residual points but there still remains a lot of noise. The result of pivoting mean filter phase loss occurs in the dense fringe regions; however, it only takes 12.6940 s. The result of the Goldstein filter is better than that of the Lee filter, which removes 99.58% of the residuals and uses 139.4579 s for filtering. A total of 124 residuals are found after TS filtering, and 99.79% of these residuals are removed. The filtering time of the TS method is 54.9642 s. However, excessive smoothing still exists. The ML filter can remove 99.71% of the residuals. The filtering effect of ML filter is better than that of the previous two, but it takes 850.2027 s to filter the entire process; the filtering efficiency is relatively low. Our proposed method removes 99.82% of the residuals, leaves only 106 residuals and consumes 266.3910 s. The proposed method is more accurate and efficiency than the traditional methods.

As shown in Fig. 6 is the enlarged region marked by black rectangle shown in Fig. 5. The Lee filter has significant noise residuals and phase loss in the black square in Fig. 6(a). The pivoting mean filter can effectively remove the noise but fail to the phase preservation in the fringe density regions in the Fig. 6(b). The result of the Goldstein filter is better than the pivoting mean filter but there is still phase loss in the fringe density regions in the Fig. 6(c). Although TS filtering has a good filtering effect, the edges of the fringe have poor retention. The phase preservation of the fringe density regions is also poor. As shown in Figs. 6(e) and 6(f), the effects of the ML filter and the proposed method are similar, but the proposed method has better phase preservation than the ML filter in the fringe density regions.

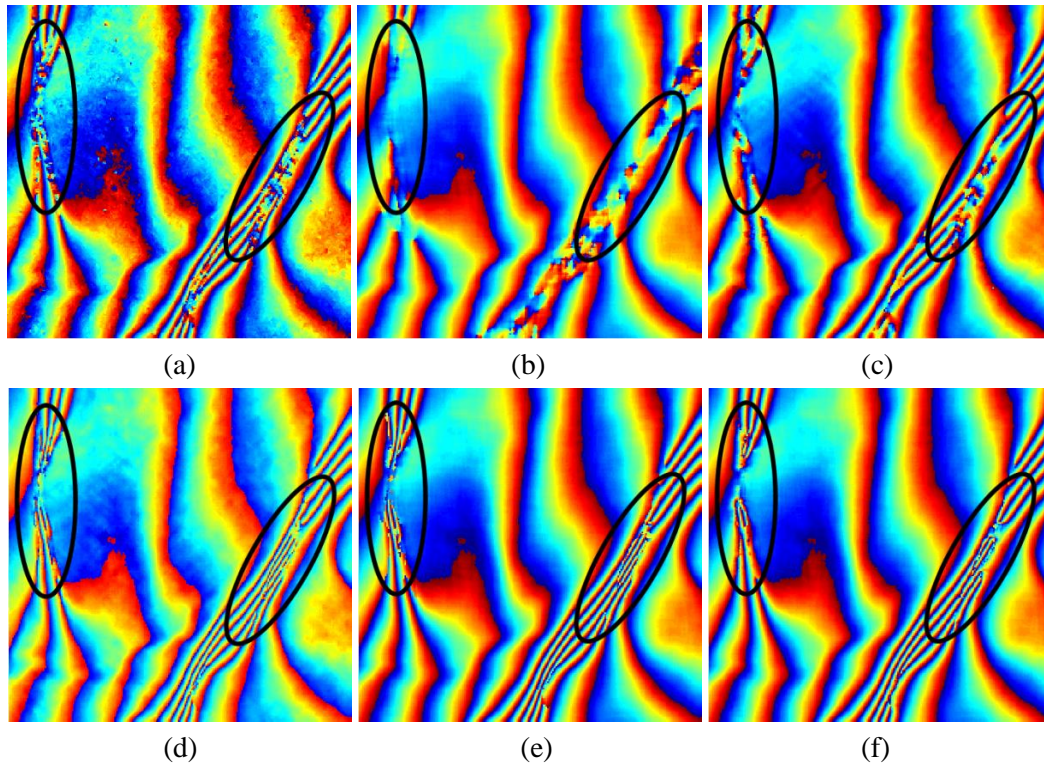


Figure 6: The enlarged region marked by black rectangle shown in Fig. 2. (a) Lee filter. (b) Pivoting mean filter. (c) Goldstein filter ($\alpha=0.5$). (d) TS filter. (e) ML filter. (f) The proposed method

As shown in Fig. 7, two sections of the section data A and B are intercepted in the real data. The experiment contrasts the Lee filter, the pivoting mean filter, the Goldstein filter, the TS filter, the ML filter, and our proposed method. In Fig. 4(a), we can see that section A is in a fringe sparsely region. Therefore, it can be seen in Fig. 7(a) that the cross section data of different filtering methods are not much different. However, section A is found in the fringe density regions. The corresponding cross-section in Fig. 7(b) reveals considerable differences among the results of the different filtering methods. The cross-sections of the Lee filter, the pivoting mean filter, and the Goldstein filter exhibit remarkable undulation. TS filter method produces substantial phase loss due to excessive smoothing. The cross sections of the ML filter and our proposed method are nearly overlapping. The proposed method is smoother than the others methods. It further proving that our proposed method has better filtering accuracy.

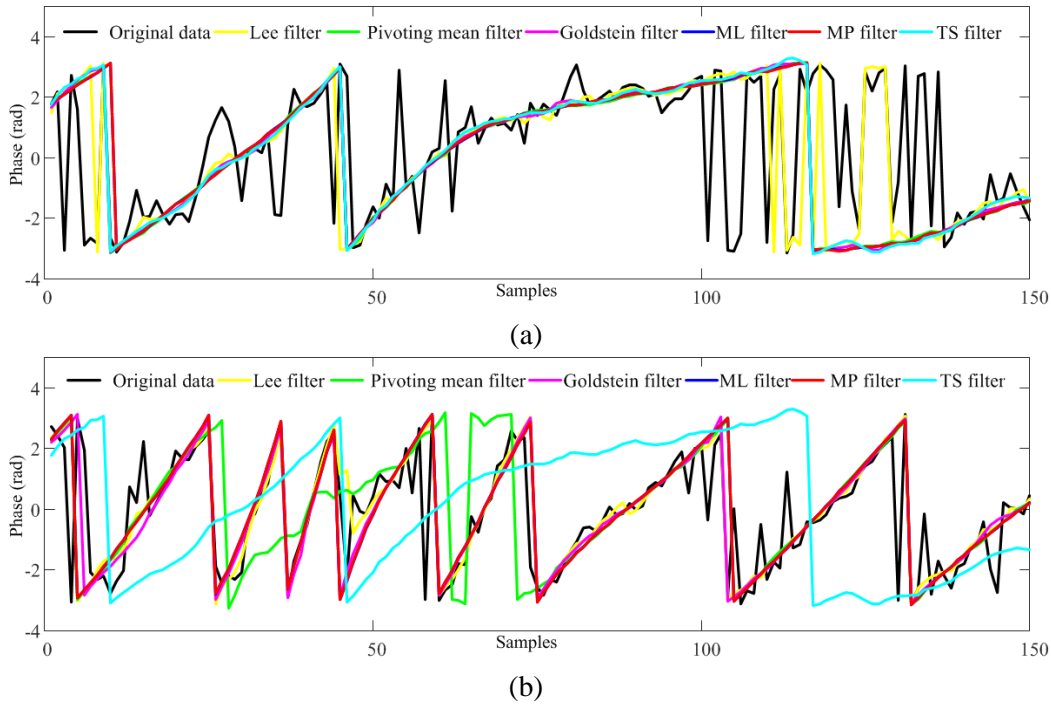


Figure 7: Two cross section data of real data. (a) The cross section data of Fig. 4(a). (b) The cross section data of Fig. 4(a)

5 Conclusions

In this letter, an interferometric phase filtering is proposed based on the amended matrix pencil and the linear window mean filter. The proposed method first transforms the interferometric phase filter into a frequency estimation problem. Then, the local frequency is estimated by an amended pencil through a simple calculation but with high precision. Finally, linear window mean filtering is used to recover the filtering phase. This method obtains the final filter phase by estimating the local frequency. The local frequency can reflect topographic changes, so even the method proposed in the fringe density regions can still obtain better results. Moreover, the proposed method only uses a simple matrix calculation to estimate the local frequency, so the method has higher computational efficiency. The Lee filter, the pivoting mean filter, the Goldstein filter, TS filter and the ML filter are compared based on simulation and real data experiments. The results show that our proposed method is more accurate and efficient than traditional methods, particularly in regions of fringe density and low coherence.

Acknowledgement: The authors would like to thank the support by the State Key Program of National Natural Science Foundation of China under Grant [Number 41774026]; the Satellite Mapping Technology and Application, National Administration of Surveying, Mapping and Geoinformation Key Laboratory under Grant [Number KLSMTA-201708].

References

- Buades, A.; Coll B.; Morel, J. M.** (2005): A non-local algorithm for image denoising. *IEEE Computer Society Conference on Computer Vision and Pattern Recognition*, vol. 2, no. 7, pp. 60-65.
- Baran, I.; Stewart, M. P.; Kampes, B. M.; Perski, Z.; Lilly, P.** (2003): A modification to the Goldstein radar interferogram filter. *IEEE Transactions on Geoscience and Remote Sensing*, vol. 41, no. 9, pp. 2114-2118.
- Cao, N.; Yu, H. W.; Lee, H.** (2018): A multibaseline InSAR phase unwrapping method using designed optimal baselines obtained by motion compensation algorithm. *IEEE Geoscience and Remote Sensing Letters*, vol. 15, no. 8, pp. 1219-1223.
- Chierchia, G.; Gheche, M. El.; Scarpa, G.; Verdoliva, L.** (2017): Multitemporal SAR image despeckling based on block-matching and collaborative filtering. *IEEE Transactions on Geoscience and Remote Sensing*, vol. 55, no. 10, pp. 5467-5480.
- Deledalle, C. A.; Denis, L.; Tupin, F.** (2009): Iterative weighted maximum likelihood denoising with probabilistic patch-based weights. *IEEE Transactions on Geoscience and Remote Sensing*, vol. 18, no. 12, pp. 2661-2672.
- Eichel, P. H.; Ghiglia, D. C.** (1993): Spotlight SAR interferometry for terrain elevation mapping and interferometric change detection. *Office of Scientific and Technical Technical Reports, SAND-93*.
- Gao, X. M.; Liu, Y. L.; Li, T.; Wu, D. Q.** (2017): High precision DEM generation algorithm based on InSAR multi-look iteration. *Remote Sensing*, vol. 9, no. 7, pp. 741-760.
- Goldstein, R. M.; Werner, C. L.** (1998): Radar interferogram filtering for geophysical applications. *Geophysical Research Letters*, vol. 25, no. 21, pp. 4035-4038.
- Hua, Y. B.** (1992): Estimating two-dimensional frequencies by matrix enhancement and matrix pencil. *IEEE Transactions on Signal Processing*, vol. 40, no. 9, pp. 2267-2280.
- Huang, B. S.; Xu, J. D.** (2008): A locally adaptive filter for noise filtering of InSAR interferogram. *Intelligent Networks and Intelligent Systems*, pp. 573-576.
- Jiang, M.; Ding, X. L.; Li, Z. W.; Tian, X.; Zhu, W. et al.** (2014): The improvement for baran phase filter derived from unbiased InSAR coherence. *IEEE Journal of Selected Topics in Applied Earth Observations and Remote Sensing*, vol. 7, no. 7, pp. 3002-3009.
- Jiang, M.; Ding, X. L.; Tian, X.; Malhotra, R.; Kong, W. X.** (2014): A hybrid method for optimization of the adaptive Goldstein filter. *ISPRS Journal of Photogrammetry and Remote Sensing*, vol. 98, pp. 29-43.
- Lanari, R.; Fornaro, G.; Riccio, D.; Migliaccio, M.; Papathanassiou, K. P. et al.** (1996): Generation of digital elevation models by using sir-c/x-sar multifrequency two-pass interferometry: the etna case study. *IEEE Transactions on Geoscience and Remote Sensing*, vol. 34, no. 5, pp. 1097-1114.
- Lee, J. S.; Papathanassiou, K. P.; Ainsworth, T. L.; Grunes, M. R.; Reigber, A.** (1998): A new technique for noise filtering of SAR interferometric phase images. *IEEE Transactions on Geoscience and Remote Sensing*, vol. 36, no. 5, pp. 1456-1465.
- Li, Z. W.; Ding, X. L.; Huang, C.; Zhu, J. J.; Chen, Y. L.** (2008): Improved filtering parameter determination for the Goldstein radar interferogram filter. *ISPRS Journal of*

Photogrammetry and Remote Sensing, vol. 63, no. 6, pp. 621-34.

Rouquette, S.; Najim, M. (2001): Estimation of frequencies and damping factors by two-dimensional esprit type methods. *IEEE Transactions on Signal Processing*, vol. 49, no. 1, pp. 237-245.

Song, R.; Guo, H. D.; Liu, G.; Perski, Z.; Fan, J. H. (2014): Improved Goldstein SAR interferogram filter based on empirical mode decomposition. *IEEE Geoscience and Remote Sensing Letters*, vol. 11, no. 2, pp. 399-403.

Spagnolini, U. (1995): 2-D phase unwrapping and instantaneous frequency estimation. *IEEE Transactions on Geoscience and Remote Sensing*, vol. 33, no. 3, pp. 579-589.

Suo, Z. Y.; Li, Z. F.; Bao, Z. (2010): A new strategy to estimate local fringe frequencies for InSAR phase noise reduction. *IEEE Geoscience and Remote Sensing Letters*, vol. 7, no. 4, pp. 771-775.

Trouve, E.; Nicolas, J. M.; Maitre, H. (1998): Improving phase unwrapping techniques by the use of local frequency estimates. *IEEE Geoscience and Remote Sensing Letters*, vol. 36, no. 6, pp. 1963-1972.

Wang, Q. S.; Huang, H. F.; Yu, A. X.; Dong, Z. (2011): An efficient and adaptive approach for noise filtering of SAR interferometric phase images. *IEEE Geoscience and Remote Sensing Letters*, vol. 8, no. 6, pp. 1140-1144.

Yu, H.; Lan, Y.; Xu, J.; An, D.; Lee, H. (2017): Large-Scale L^0 -Norm and L^1 -Norm 2-D phase unwrapping. *IEEE Transactions on Geoscience and Remote Sensing*, vol. 55, no. 8, pp. 4712-4728.

Yu, H. W.; Lee, H.; Yuan, T.; Cao, N. (2018): A novel method for deformation estimation based on multibaseline InSAR phase unwrapping. *IEEE Transactions on Geoscience and Remote Sensing*, vol. 56, no. 9, pp. 1-13.

Zhang, W. G.; Zhang, Q.; Zhao, C. Y.; Yang, C. S.; Zou, W. B. (2014): Noise reduction for InSAR phase images using BM3D. *Chinese Journal of Electronics*, vol. 23, no. 2, pp. 329-333.

Zhao, W. S.; Jiang, M.; He, X. F. (2016): Improved adaptive Goldstein interferogram filter based on second kind statistics. *Acta of Geodaetica Cartographica Sinica*, vol. 45, no. 10, pp. 1200-1209.